Supplementary Information of

Furfural Exhibits Distinct Photooxidation and Secondary Organic Aerosol Formation Among Biomass Burning Related Furanoids

Taekyu Joo et al.

Correspondence to: Taekyu Joo (taekyujoo@korea.ac.kr) and Nga L. Ng (ng@caltech.edu)

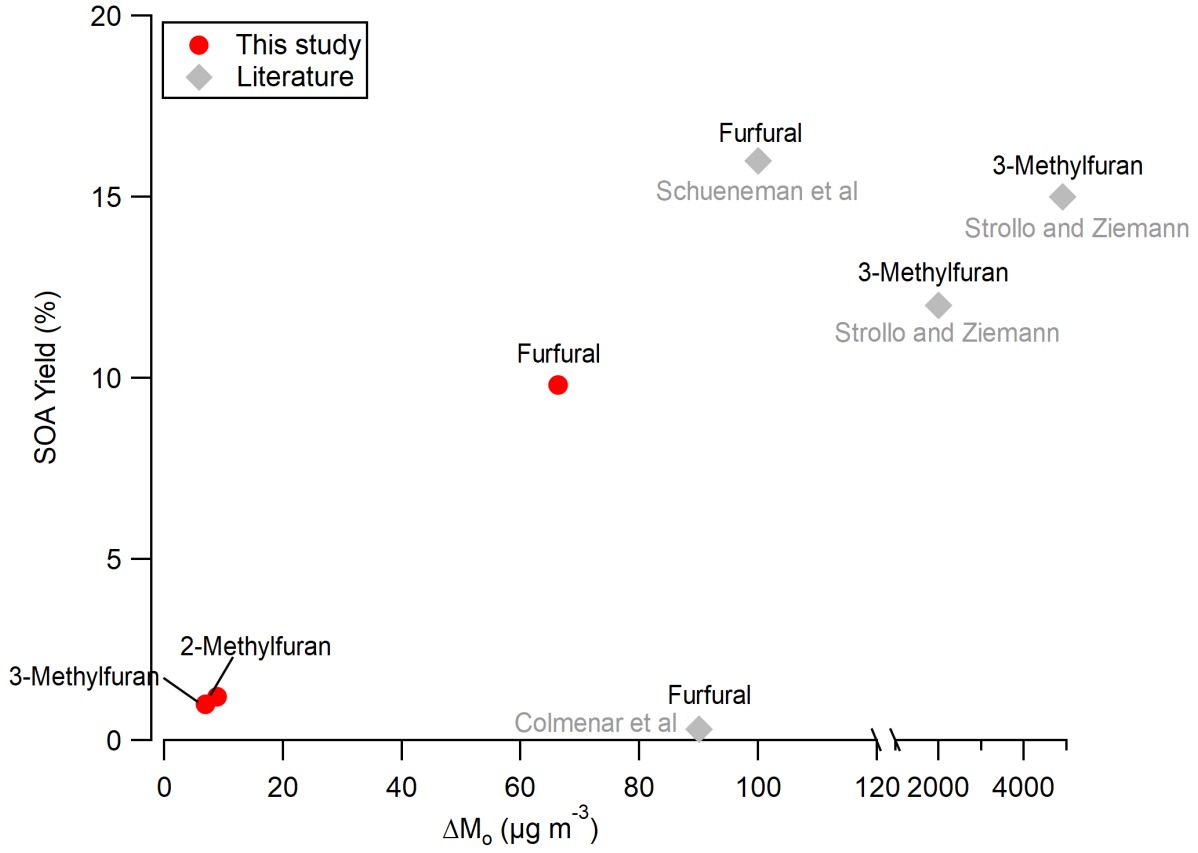

Figure S1. SOA yields of furanoid+OH are compared with previously reported values. Red markers refer to values obtained in the current study, and gray markers represent literature values (Schueneman et al., 2024; Strollo and Ziemann, 2013; Colmenar et al., 2020).

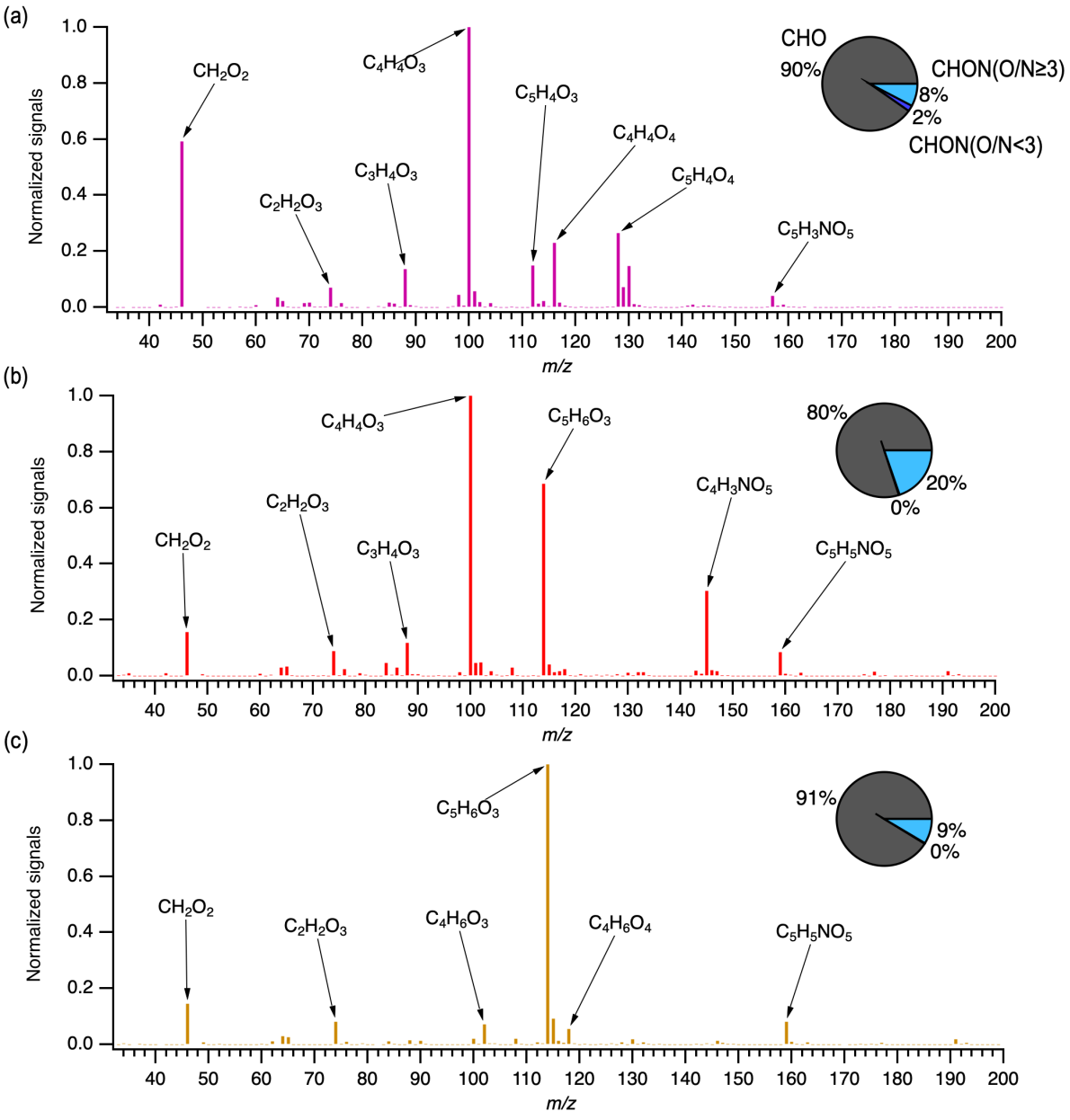

Figure S2. Gas-phase mass spectra of (a) furfural+OH, (b) 2-methylfuran+OH, and (c) 3-methylfuran+OH experiments measured using HR-ToF-CIMS.

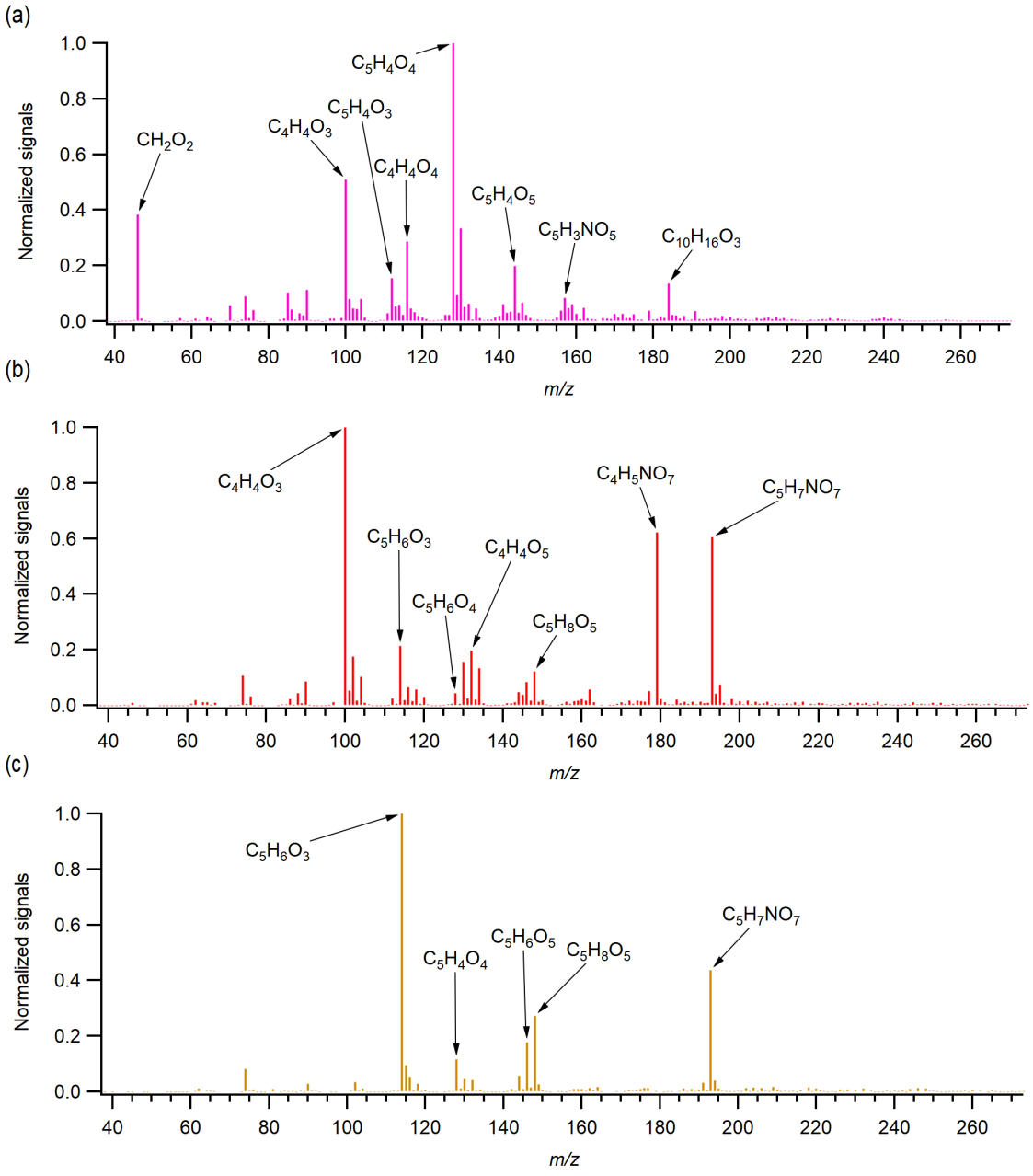

Figure S3. Particle-phase mass spectra of (a) furfural SOA, (b) 2-methylfuran SOA, and (c) 3-methylfuran SOA measured using FIGAERO-CIMS.

(a)

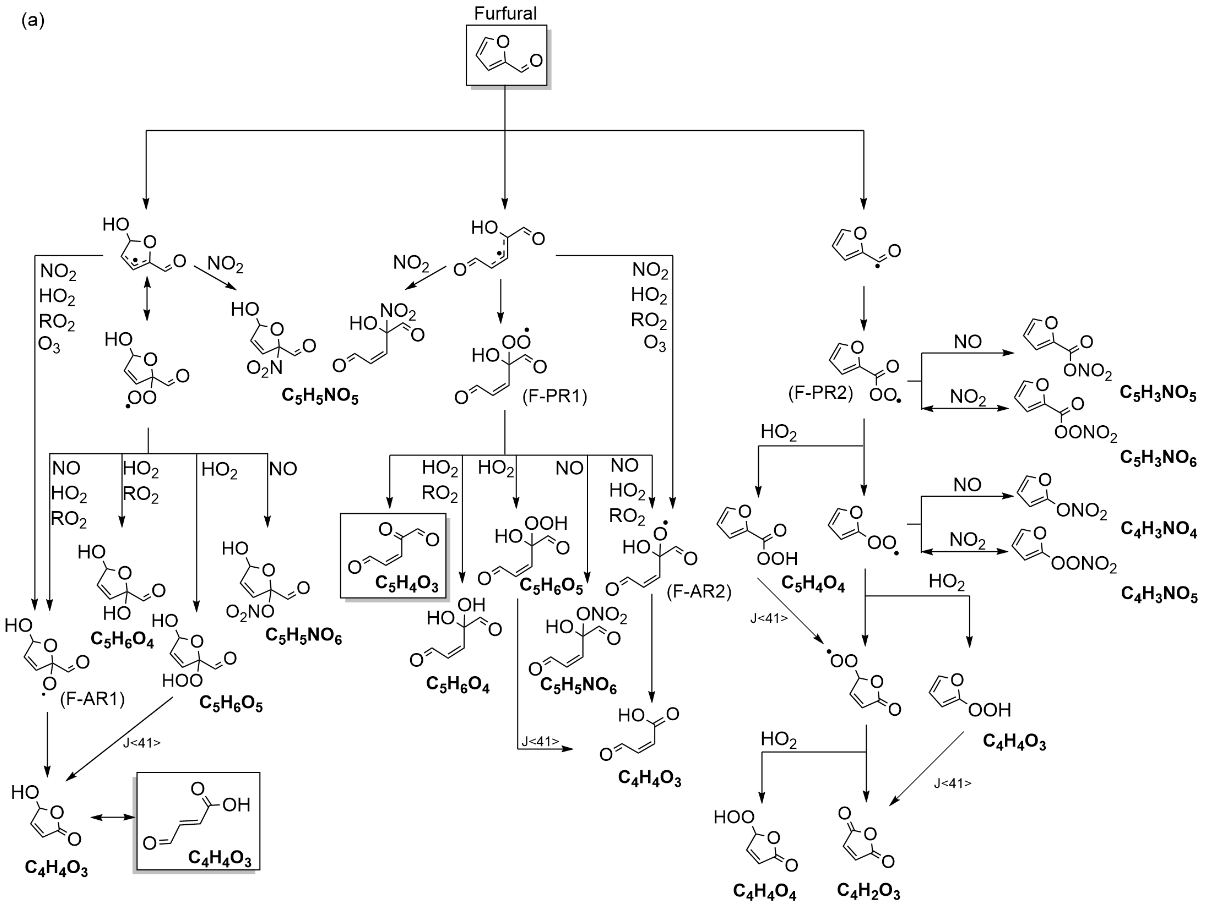

Furfural
NO2
HO2
RO2
O3
NO
(F-PR1)
(F-PR2)
(F-AR1)
(F-AR2)
J<41>
C5H5NO5
C5H6O4
C5H5NO6
C5H6O5
C5H4O3
C5H3NO5
C5H3NO6
C4H3NO4
C4H3NO5
C5H4O4
C4H4O3
C4H4O4
C4H2O3

(a-i)

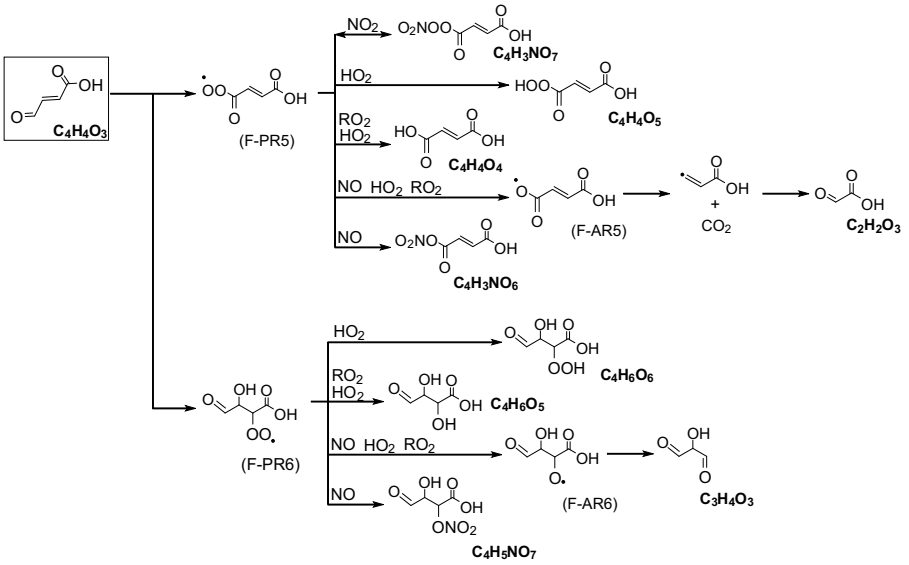
C4H4O3
(F-PR5)
NO2
O2NOO
C4H3NO7
HO2
HOO
C4H4O5
RO2
HO2
HO
C4H4O4
NO HO2 RO2
(F-AR5)
CO2
C2H2O3
NO
O2NO
C4H3NO6
(F-PR6)
HO2
C4H6O6
RO2
HO2
C4H6O5
NO HO2 RO2
(F-AR6)
C3H4O3
NO
ONO2
C4H5NO7

(a-ii)

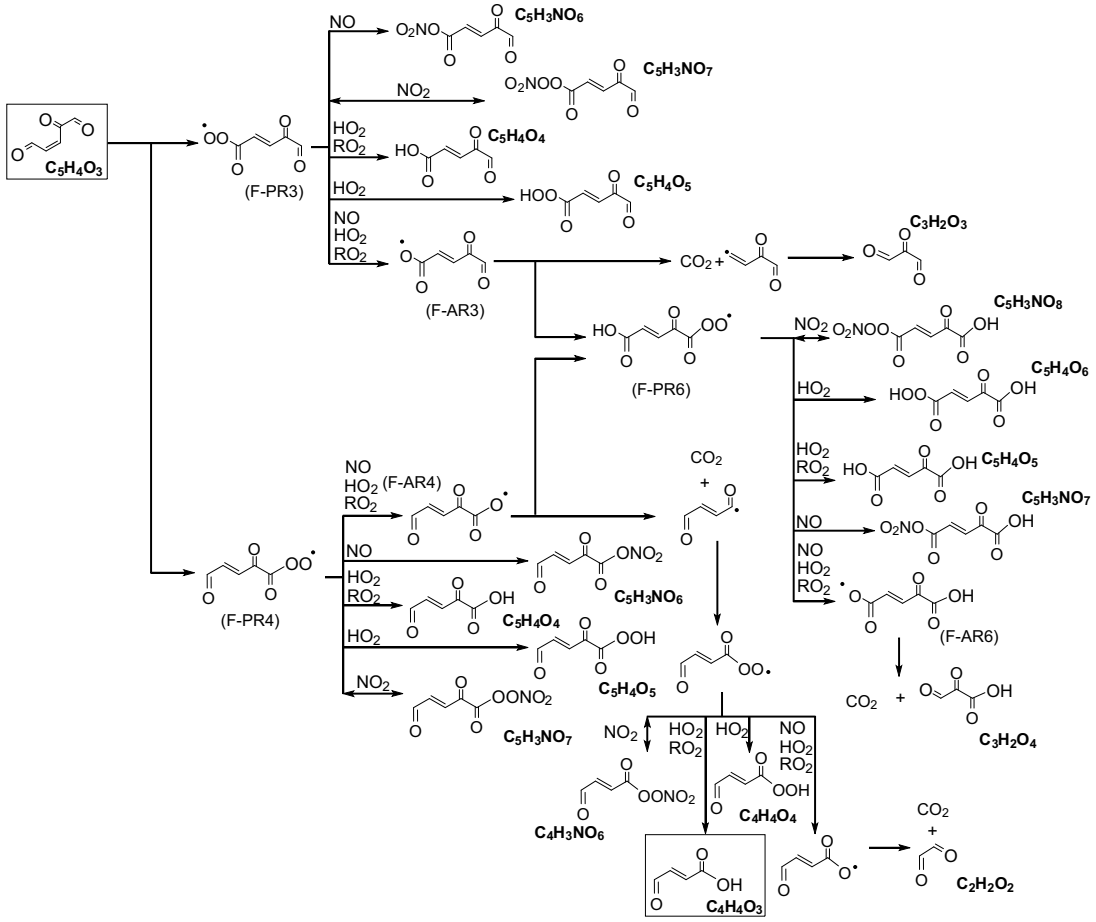
C5H4O3
(F-PR3)
NO
NO2
HO2
RO2
C5H3NO6
C5H3NO7
C5H4O4
C5H4O5
(F-AR3)
C3H2O3
CO2
(F-PR6)
C5H3NO8
C5H4O6
(F-PR4)
(F-AR4)
(F-AR6)
C5H3NO6
C5H4O4
C5H4O5
C5H3NO7
C3H2O4
C4H3NO6
C4H4O4
C4H4O3
C2H2O2

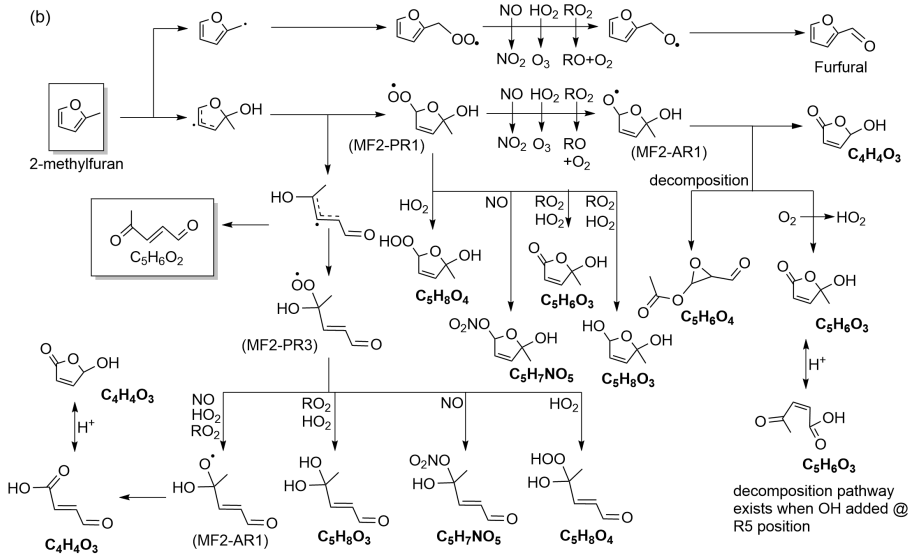
(b)
2-methylfuran
Furfural
(MF2-PR1)
(MF2-AR1)
(MF2-PR3)
decomposition
decomposition pathway exists when OH added @ R5 position

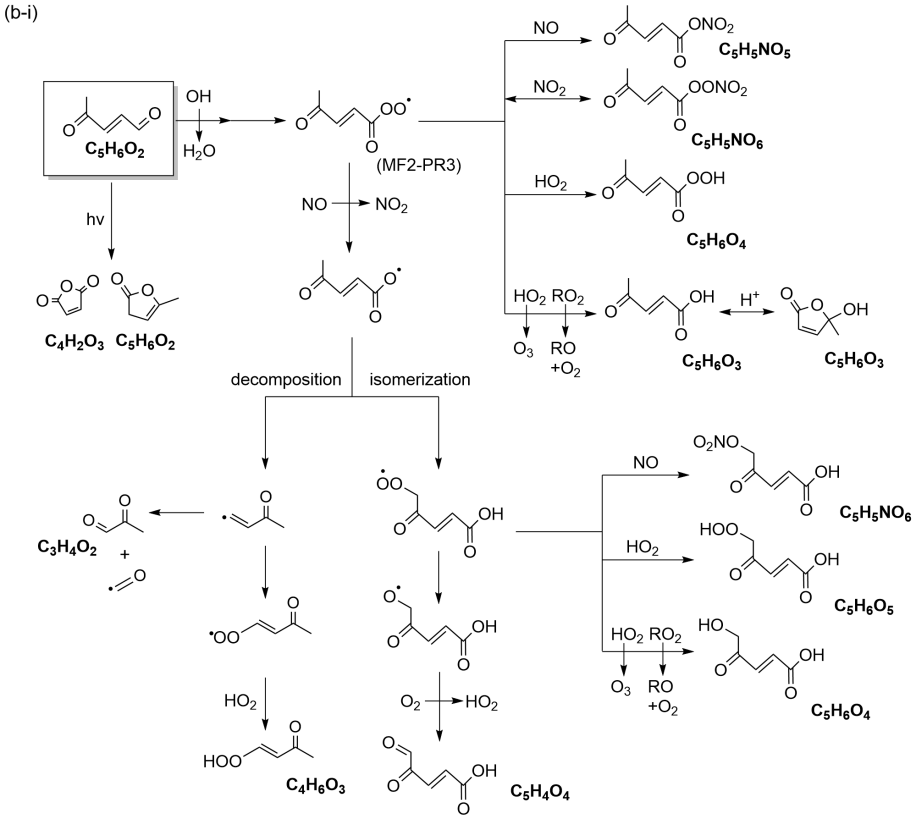
(b-i)
(MF2-PR3)
hv
decomposition
isomerization

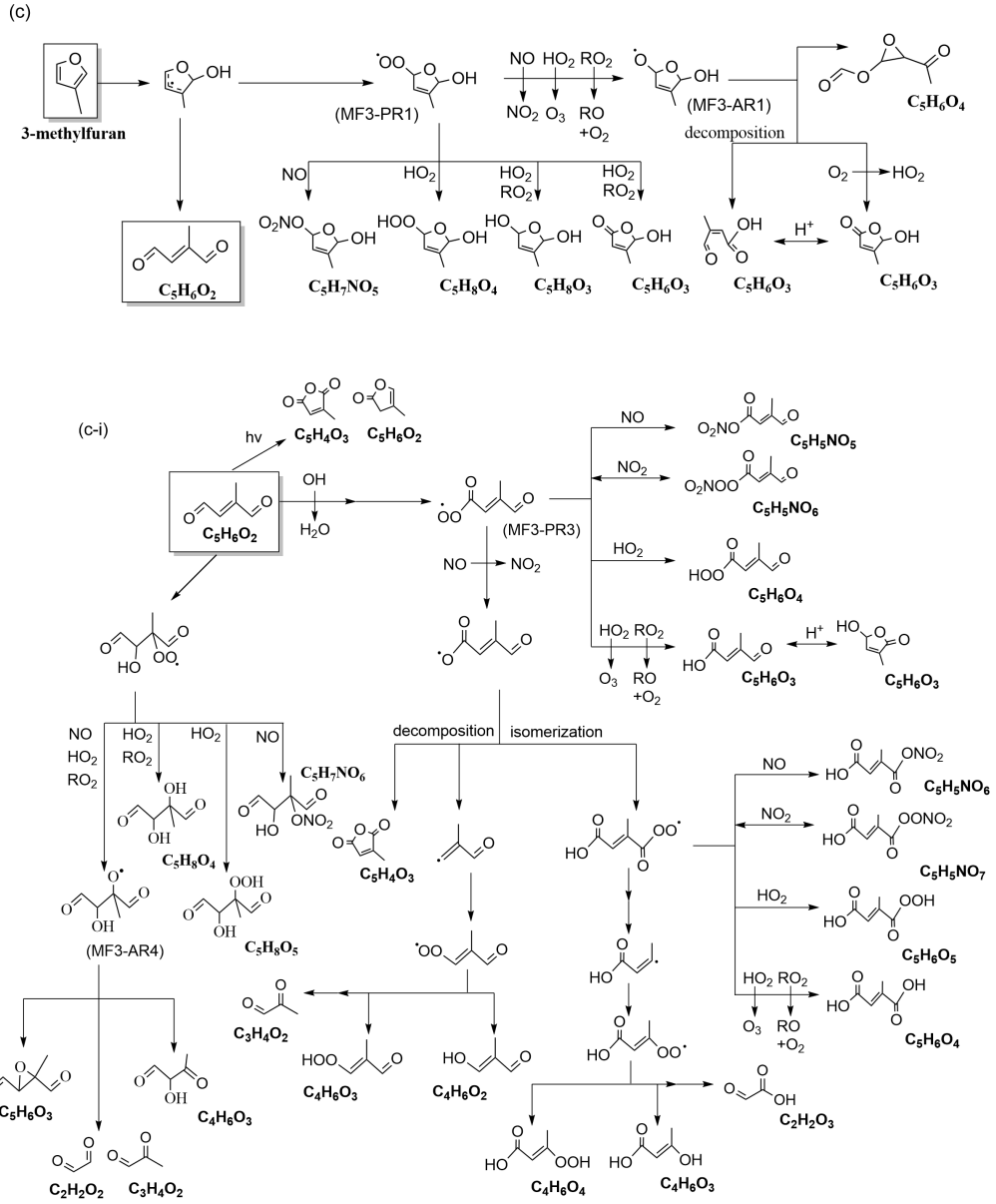

Figure S4. Extended oxidation mechanisms of (a) furfural+OH, (b) 2-methylfuran+OH, and (c) 3-methylfuran+OH. Multigenerational oxidation pathways of major ring-opened first-generation products (boxed species) of (a) furfural+OH, (b) 2-methylfuran+OH, and (c) 3-methylfuran+OH reactions are shown in (a-i and ii), (b-i), and (c-i), respectively. Species proposed here are identified from HR-ToF-CIMS.

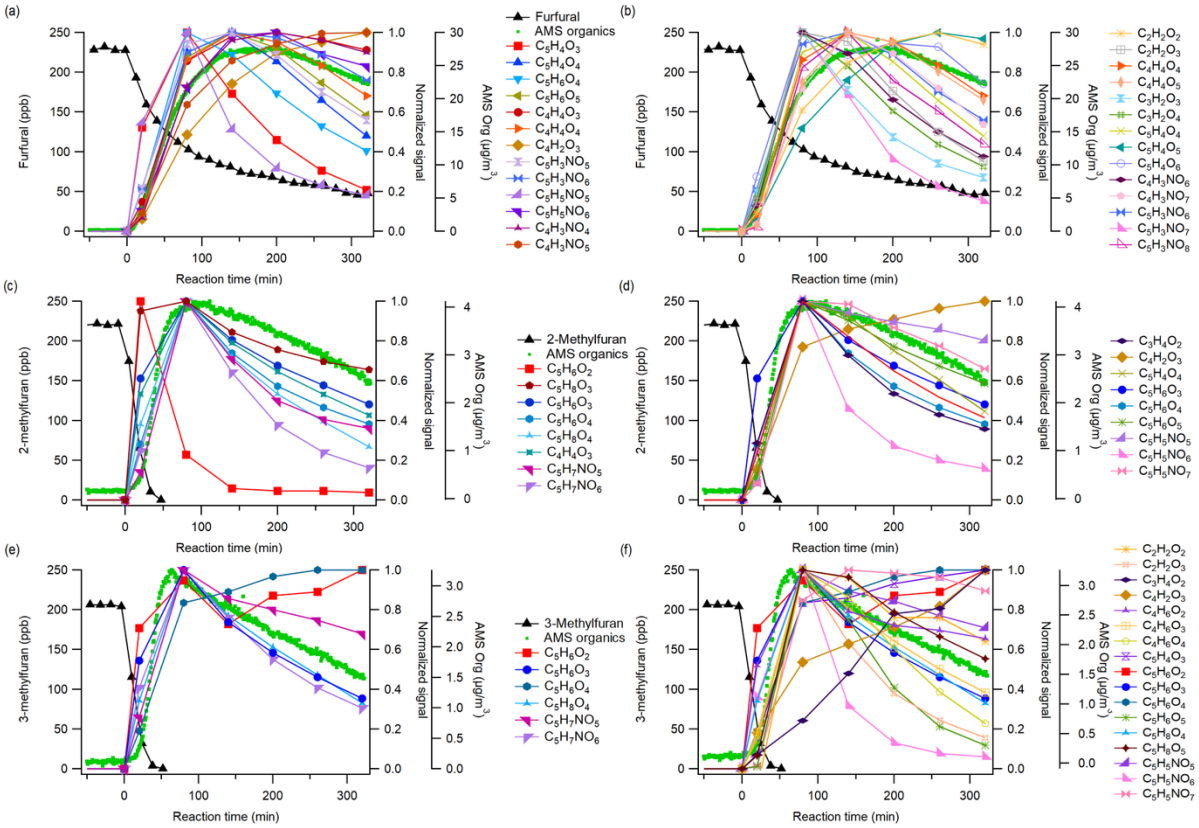

Figure S5. Temporal profiles of precursor VOCs with gas-phase oxidation products and organic aerosol during (a, b) furfural+OH, (c, d) 2-methylfuran+OH, and (e, f) 3-methylfuran+OH reactions measured by HR-ToF-CIMS. Compounds listed in this figure include oxidation products that are proposed in the detailed mechanism in Figure S4. Figures in the left panel (a, c, e) are temporal profiles of first-generation products, and the figures in the right panel (b, d, f) are temporal profiles of second or later-generation products.

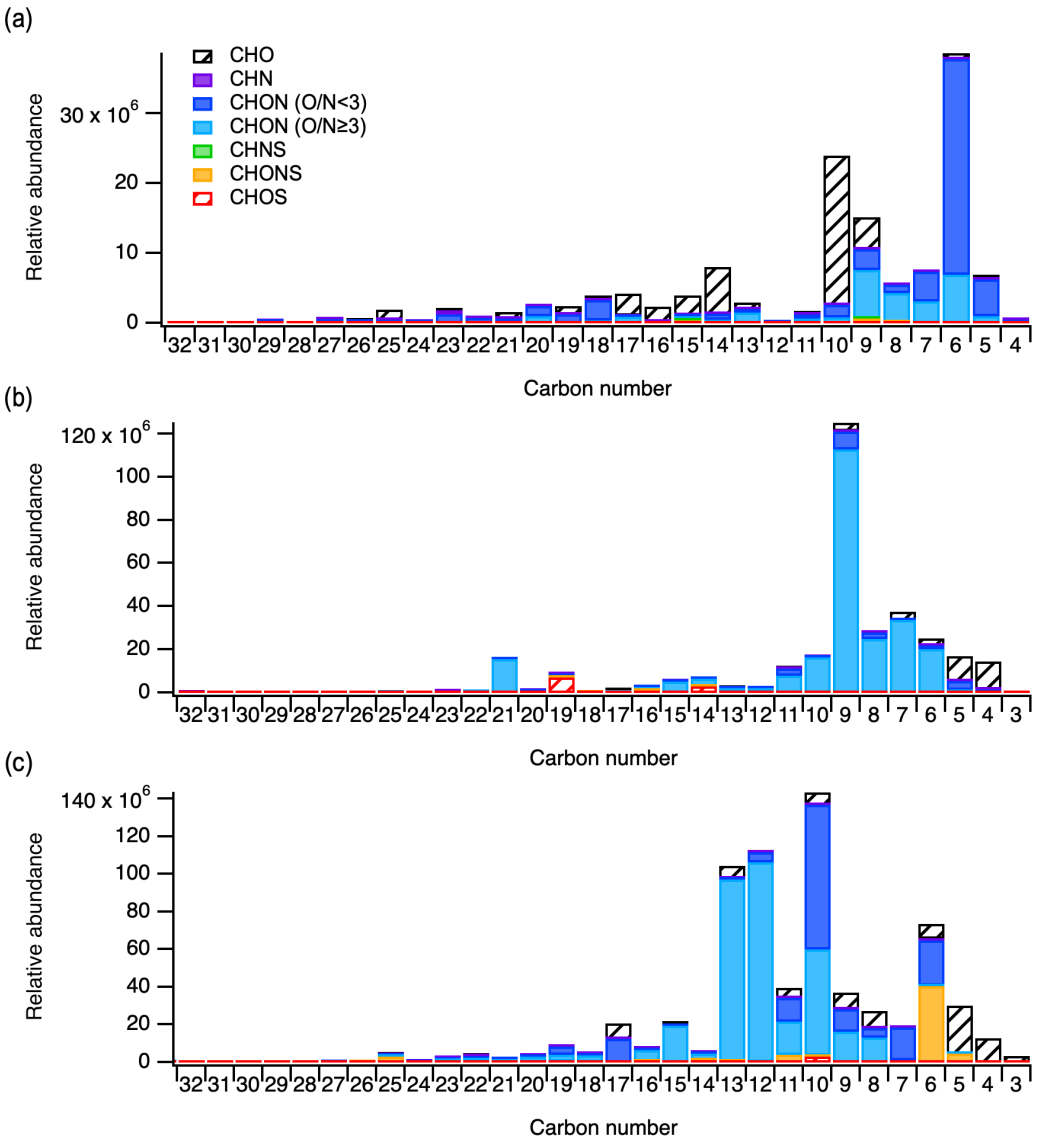

Figure S6. Non-targeted LC-ESI-Q-ToF analysis results of (a) furfural SOA (reproduced from Joo et al. (2024)), (b) 2-methylfuran SOA, and (c) 3-methylfuran SOA showing carbon number of identified compounds, color coded by compound class. The difference in compound class distributions between FIGAERO-CIMS (Figure 7 in the main text) and LC-ESI-Q-ToF are expected based on differences in ionization chemistry, choice of column, and polarity of ionization between the two methods.

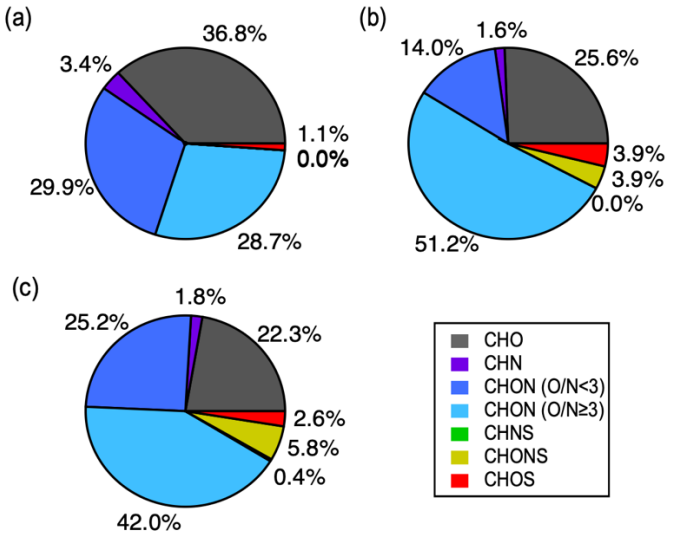

Figure S7. Distributions of number of distinct compounds identified in (a) furfural SOA, (b) 2-methylfuran SOA, and (c) 3-methylfuran SOA via LC-ESI-Q-ToF. The results show higher relatively higher contribution of CHON species with O/N≥3 in 2- and 3-methylfuran SOA than in furfural SOA, suggesting a great number of organic nitrate compounds are likely present in 2- and 3-methylfuran SOA. The difference in compound class distributions between FIGAERO-CIMS (Figure 7 in the main text) and LC-ESI-Q-ToF are expected based on differences in ionization chemistry, choice of column, and polarity of ionization between the two methods.

Table S1. Additional experiments with higher initial VOC concentrations to facilitate collection of sufficient aerosol mass for filter sampling and LC-ESI-Q-ToF analysis. Experimental conditions in this table are identical to those reported in Joo et al. (2024).

Exp.	Precursor	Initial NO_x (ppb)	RH (%)	Injected VOC (ppb)*	ΔVOC (ppb)*	ΔM_o (μg m^{-3})**	Yield (%)
4	Furfural	576	< 5	294.8 ± 6.3	212.4 ± 6.3	96.1±1.5	11.5±0.3
5	2-methylfuran	734	< 5	537.0 ± 7.1	537.0 ± 7.1	49.9±0.8	2.8±0.05
6	3-methylfuran	964	< 5	629.2 ± 9.5	629.2 ± 9.5	113.8±1.8	5.4±0.1

* Uncertainties of VOC and consumed VOC (ΔVOC) are calculated based on the GC-FID calibration error and 1σ of VOC concentrations before onset of the photooxidation.

** Uncertainties for ΔM_o are calculated from 1σ of aerosol volume concentration measured by the SMPS during peak SOA mass concentration. Uncertainties in the SOA density are also propagated.

Table S2. R_{ON} (organic nitrate NO^+/NO_2^+) and R_{ON}/R_{AN} ratio of furanoid SOA estimated from HR-ToF-AMS. R_{AN} (ammonium nitrate NO^+/NO_2^+) value of 2.44 is obtained during ionization efficiency calibration of HR-ToF-AMS.

Exp.	Precursor	R_{ON}	R_{ON}/R_{AN}
1	Furfural	6.75	2.77
2	2-methylfuran	5.15	2.11
3	3-methylfuran	5.50	2.25

References

Colmenar, I., Martín, P., Cabañas, B., Salgado, S., Villanueva, F., and Ballesteros, B.: Evaluation of the SOA Formation in the Reaction of Furfural with Atmospheric Oxidants, Atmosphere, 11, 927, 2020.

Joo, T., Machesky, J. E., Zeng, L., Hass-Mitchell, T., Weber, R. J., Gentner, D. R., and Ng, N. L.: Secondary Brown Carbon Formation From Photooxidation of Furans From Biomass Burning, Geophysical Research Letters, 51, e2023GL104900, https://doi.org/10.1029/2023GL104900, 2024.

Schueneman, M. K., Day, D. A., Peng, Z., Pagonis, D., Jenks, O. J., de Gouw, J. A., and Jimenez, J. L.: Secondary Organic Aerosol Formation from the OH Oxidation of Phenol, Catechol, Styrene, Furfural, and Methyl Furfural, ACS Earth and Space Chemistry, 8, 1179-1192, 10.1021/acsearthspacechem.3c00361, 2024.

Strollo, C. M. and Ziemann, P. J.: Products and mechanism of secondary organic aerosol formation from the reaction of 3-methylfuran with OH radicals in the presence of NOx, Atmospheric Environment, 77, 534-543, https://doi.org/10.1016/j.atmosenv.2013.05.033, 2013.